Robust Model Predictive Direct Speed Control for SPMSM Drives Based on Full Parameter Disturbances and Load Observer

Xiaoguang Zhang, *Member, IEEE*, Yu Cheng, Zhihao Zhao, and Yikang He

***Abstract*—A robust model-predictive direct-speed control (MP-DSC) for the surface-mounted permanent-magnet synchronous motor (SPMSM) drives is proposed in this article. First, MP-DSC based on direct voltage-selection cost function is introduced. Then, a sliding-model full parameter disturbances and load observer (FPLO) that can simultaneously estimate electrical parameter disturbances, mechanical parameter disturbances, voltage reconstruction error, motor speed, and load torque is proposed. Thus, the load torque observer in the conventional MP-DSC method is eliminated. Then, the MP-DSC+FPLO method is presented, in which the output of the proposed FPLO is used to compensate for the predicted reference voltage error. The simulation and experimental results show that the proposed method is robust to the disturbance of parameters and load.**

***Index Terms*—Direct speed control (DSC), parameter sensitivity, sliding-model observer (SMO).**

I. Introduction

MODEL predictive control (MPC) is a nonlinear control method. Compared with conventional motor control methods such as field-oriented control [1], [2], and direct torque control (DTC) [3], [4], MPC method is simpler in structure, more intuitive in concept, and easier to implement. With the above merits, the application of MPC technology in the field of power electronics and power transmission has attracted more and more attention [5], [6].

Finite control set model predictive speed control (MPSC) is one of MPC. In the MPSC, the discrete models of inverter and motor are used to predict the motor speed and current, and a quality function based on tracking the reference speed and current is constructed to select the optimal voltage vector so as to achieve the optimal control [7], [8]. On the advantages side, the MPSC strategy has the characteristics of good dynamic performance. Moreover, the speed PI control loop normally used in conventional model predictive current control (MPCC)/model predictive torque and flux control (MPTC) is omitted in MPSC. However, similar to the other model-based control strategies (such as MPCC method/MPTC method), the performances of the MPSC method highly depend on precise model parameters [9]. Therefore, the parameter value used in the MPSC (inductance, resistance, flux linkage, moment of inertia, and load disturbance) needs to be consistent with the actual parameter value to achieve good dynamic and steady-state control performance. In fact, when the motor operates in different states, the motor parameter will change accordingly; additionally, the unknown disturbance inevitably exists in the system operating environment, which makes it difficult to keep the system parameters consistent with the actual values [10]. In order to improve the robustness of the control system, many solutions have been proposed, including the parameter identification method [11]–[14], incremental model-based method [15], [16], observer-based method [18]–[24], and else.

The parameter identification algorithm is usually adopted to improve the permanent-magnet synchronous motor (PMSM) control system robustness when parameter error or mismatch exists. In [11], the PMSM flux linkage is identified from the speed harmonics, which diminishes the steady-state tracking bias caused by flux linkage mismatch. In [12], the addition of position offsets is used to estimate the rotor flux linkage without the nominal parameter values of the motor. Experiments show that the method has very high accuracy in flux linkage identification. Besides, in the literature [13], a novel predictive current control algorithm is proposed to reduce the current oscillation by identifying the inductance value. A quantum genetic algorithm, which can ensure all parameters are identifiable, is introduced in [14].

In addition, an incremental model-based method is considered as a more effective solution for improving robustness, since the flux linkage parameter is eliminated from the current prediction model. In [15], a robust predictive current control algorithm for PMSM is presented. The incremental system model is adopted to solve the robustness issue of flux linkage parameter, and the inductance robustness is increased by adding an extended state observer. In [16], the influence mechanism of electrical

Manuscript received May 12, 2019; revised October 30, 2019; accepted December 25, 2019. Date of publication December 29, 2019; date of current version April 22, 2020. This work was supported in part by the National Natural Science Foundation of China under Grant 51877002, in part by Beijing Natural Science Foundation under Grant 3172011, in part by the Outstanding Young Scholars Fund of North China University of Technology, in part by the Young TopNotch Talents Program of Beijing Excellent Talents Funding (2017000026833ZK12), in part by the Fundamental Research Funds for Beijing Universities under Project 110052971921/025, in part by the Young TopNotch Talents Program for Municipal Universities of Beijing (CIT&TCD201904011), and in part by the 2019 Beijing Nova Program (Z191100001119036). Recommended for publication by Associate Editor H. Hofmann. *(Corresponding author: Xiaoguang Zhang.)*

The authors are with the North China University of Technology, Beijing 100144, China (e-mail: zhangxg123456789@163.com; 625632961@qq.com; 1434376387@qq.com; he-yk@qq.com).

Color versions of one or more of the figures in this article are available online at http://ieeexplore.ieee.org.

Digital Object Identifier 10.1109/TPEL.2019.2962857

parameter error on the current control performance is revealed, and an inductance extraction algorithm is proposed based on the incremental model.

Recently, an observer-based control strategy has been considered as a good method to solve the problems of parameter mismatch or load disturbance [17]–[21]. In these observers, sliding-mode observer (SMO) receives wide attention because of its strong robustness advantage. Especially in the estimation of key parameters and variables, SMOs are widely adopted. In [28], a sliding-mode flux observer is proposed to improve the DTC performance of IPMSM at low speed. Different from other flux observers, this observer can accurately observe flux linkage under the condition that any speed adaptation mechanism is not included. In [29] and [30], an adaptive control theory is incorporated into SMO design to observe rotor flux and speed. The super-twisting second-order SMO is developed in [31] and [32] for the identification of mechanical systems, the test results show that the observer accuracy is satisfactory. In addition to the estimation of a single parameter or variable, SMO can also be used to observe disturbances caused by multiparameter-mismatches or load change. In [23], an SMO that can observe all electrical parameter mismatches, including resistance, inductance, and flux linkage, is presented. In [33], in order to estimate multiple mechanical parameters, a terminal SMO is presented. The load torque, the friction coefficient, and the moment of inertia can be estimated sequentially by this terminal SMO.

However, usually, the load disturbance and electrical and mechanical parameter mismatches exist simultaneously in the actual system. Therefore, it is necessary to present a kind of observer which not only can observe the load torque disturbance but also observe all parameter errors (electrical and mechanical parameter errors) to improve the robustness of the whole system.

In this article, a model predictive direct speed control (MP-DSC) method with full parameter disturbances and load torque observer (MP-DSC+FPLO) is proposed. First, the reference speed and reference current of the conventional MPSC method are unified as a reference voltage vector by deadbeat control principle, then a direct-voltage-selection based cost function is designed. Furthermore, the influence of parameter mismatches, inaccurate voltage reconstruction, and load disturbance on reference voltage is investigated in this article. It can be found that all these disturbances will lead to reference voltage prediction error, which will deteriorate the control performance. In order to improve the robustness of the system, a novel full parameter disturbances and load torque observer (FPLO) is proposed. In each control cycle, the reference voltage errors caused by all parameter mismatches, inaccurate voltage reconstruction, and load disturbance can be observed online by FPLO, and then this error is compensated to obtain accurate reference voltage values. Therefore, the selected optimal voltage vector will no longer depend strictly on the precise mathematical model parameters, and the motor control system will have a good antidisturbance ability.

This article proceeds as follows. The motor model and the conversion of the reference value and the quality function are investigated in Section II. Then, Section III quantifies the influence of model parameters and load disturbance on the reference voltage. And Section IV presents the FPLO based on the principle of sliding-mode control. In addition, the MP-DSC+FPLO method is developed. In Section V, the effectiveness of the method is verified by experimental comparisons. Finally, the conclusion is given in Section VI.

II. MP-DSC Without Weighting Factor

In this section, the SPMSM mathematical model and the compensation method of one-step delay are described in stationary frame. Then, the MP-DSC method is developed.

A. SPMSM Mathematical Model

The *d*-axis equivalent inductance of SPMSM is equal to the *q*-axis equivalent inductance, which means that $L_d = L_q = L$. Then, in the *d–q* reference frame, the stator voltage and electromagnetic torque can be expressed as

$$\begin{cases} u_d = Ri_d + L\frac{di_d}{dt} - \omega L i_q \\ u_q = Ri_q + L\frac{di_q}{dt} + \omega L i_d + \omega\psi_f \end{cases} \tag{1}$$

$$T_e = \frac{3}{2}p\psi_f i_q \tag{2}$$

where u_d and u_q are the *d*- and *q*-axis stator terminal voltages; i_d and i_q are the *d*- and *q*-axis stator currents; *R* and *L* are the stator resistance and inductance; ψ_f is the magnetic flux-linkage; ω is the electrical angular velocity of the rotor; T_e is the electromagnetic torque; and *p* is the number of poles.

Moreover, the mechanical equation is expressed as

$$\frac{d\omega}{dt} = \frac{p}{J}(T_e - T_l) - \frac{1}{J}B\omega \tag{3}$$

where T_l is the load torque on the shaft of a motor; *J* is the rotor inertia; and *B* is the viscous friction coefficient.

B. One-Step Delay Compensation

According to [25], the system control performance will become bad when the one-step delay exists in the digital control. In this article, to compensate this one-step delay, the predictive current is substituted into the motor model to achieve better control performance. Therefore, based on the discretized voltage equation (1), the predicted current at $k+1$ control time can be obtained as follows [16]:

$$\begin{cases} i_d(k+1) = \left(1 - \frac{T_s R}{L}\right)\cdot i_d(k) \\ \qquad\qquad + T_s\omega(t) i_q(k) + \frac{T_s}{L}\cdot u_d(k) \\ i_q(k+1) = \left(1 - \frac{T_s R}{L}\right)\cdot i_q(k) \\ \qquad\qquad - T_s\omega(t) i_d(k) + \frac{T_s}{L}\cdot u_q(k) - \frac{T_s\omega(t)\psi_f}{L} \end{cases} \tag{4}$$

where T_s is current sampling period and $\omega(t)$ is the speed at (*t*)th instant.

Based on the predicted current described by (4) and the discretized voltage equation (1), the predicted voltage equation at $k+1$ time can be obtained as

$$\left\{ u_d(k+1) = \frac{L}{T_\mathrm{s}}\cdot i_d(k+2) + a(k+1) \right. \tag{5a}$$

$$\left\{ u_q(k+1) = \frac{L}{T_\mathrm{s}}\cdot i_q(k+2) + b(k+1) \right. \tag{5b}$$

where

$$a(k+1) = \left(R - \frac{L}{T_s}\right) \cdot i_d(k+1) - \omega(t) L i_q(k+1)$$

$$b(k+1) = \left(R - \frac{L}{T_s}\right) \cdot i_q(k+1) + \omega(t)\left[L i_d(k+1) + \psi_f\right].$$

C. Reference Conversion

In this section, reference speed information and reference current information are consolidated into reference voltage information, which can be used to construct quality function to eliminate the weighting factor existed in the conventional speed predictive control method.

First, substituting (2) into (3), the mechanical equation can be simplified as

$$\frac{d\omega}{dt} = \frac{P}{J} \cdot \left(\frac{3}{2} p \psi_f i_q - T_l\right) - \frac{1}{J} B \omega. \tag{6}$$

Then, the predicted speed is able to be obtained using the forward Euler discretization equation as

$$\omega(t+1) = \omega(t) + \frac{T_{sp} p}{J}\left[3 p \psi_f i_q(k+2)/2 - T_l\right] - \frac{T_{sp}}{J} B \omega. \tag{7}$$

It is well known that the mechanical response time of the speed regulating system is much longer than the electromagnetic response time. Therefore, the sampling time T_{sp} of mechanical variables in (7) is ten times slower than the sampling time T_s of electromagnetic variables namely, $T_{sp} = 10\,T_s$, while *t* is the sampling instant of speed and $\omega(t+1)$ represents the predicted speed.

Next, substituting (7) into (5b), the predicted speed can be converted into the q-axis predicted voltage as follows:

$$u_q(k+1) = \frac{L}{T_s} \cdot \frac{2J\left[\omega(t+1) - \omega(t)\right] + 2T_{sp} p T_l + 2T_{sp} B \omega(t)}{3 p^2 \psi_f T_{sp}} + b(k+1). \tag{8}$$

It can be known from (8) that the predicted q-axis voltage contains the predicted speed information at $(t+1)$ time. On the other hand, from (5a), it is obvious that the d-axis predicted voltage contains the d-axis predicted current information at $(k+2)$ time.

Therefore, in order to track the reference speed and reference current at the next moment, the deadbeat control principle is adopted in this work, where the predicted speed $\omega(t+1)$ is selected as reference speed ω^* and the predicted current $i_d(k+2)$ is selected as reference current i_d^*. Then, the reference voltage equation can be obtained by combining (5a) and (8) as

$$u^* = \begin{bmatrix} u_d^* \\ u_q^* \end{bmatrix} = \begin{bmatrix} \frac{L}{T_s} \cdot i_d^* + a(k+1) \\ \frac{L}{T_s} \cdot \frac{2J[\omega^* - \omega(t)] + 2T_{sp} p T_l + 2T_{sp} B \omega(t)}{3 p^2 \psi_f T_{sp}} + b(k+1) \end{bmatrix} \tag{9}$$

where u_d^* and u_q^* represent the d-and q-axis components of the reference voltage, respectively. In this article, the maximum torque current ratio strategy is adopted, namely, $i_d^* = 0$. In addition, the load torque information in (9) can be obtained by the load torque observer proposed in [26].

D. Quality Function

The primary objective of MPSC is to track the reference speed ω^* [7]. Therefore, speed error is included in the quality function of the conventional MPSC. In addition, in order to improve the efficiency and reduce the torque ripple, the d-axis current needs to be controlled near zero, while the fluctuation of the q-axis current is used as the evaluation criterion of the quality function in the conventional method. The quality function expression of the conventional MPSC can be simplified as [7]

$$G = (\omega^* - \omega)^2 + N_{id}(i_d)^2 + N_{iq}(i_{qf})^2 \tag{10}$$

where i_{qf} is the high-pass filtered q-axis current; and N_{id} and N_{iq} are the weighting coefficients, which need to be designed and tuned through a large number of experiments and simulations.

This article establishes a quality function without weighting factor based on the reference voltage $u*$, which is shown as follows:

$$Q = \left(u^* - u_s^i\right)^2 \tag{11}$$

where u_s^i is the candidate voltage vector, which can be obtained from eight basic voltage vectors of the two-level inverter. The candidate voltage vector that has the minimum quality function should be chosen as the optimal voltage vector. Equation (11) can also be expressed as follows:

$$Q = \left(u_d^* - u_d^i\right)^2 + \left(u_q^* - u_q^i\right)^2 \tag{12}$$

where u_d^i and u_q^i represent the d-axis and q-axis components of candidate voltage, respectively.

In order to analyze the control relationship between this method and the conventional method, the following extended expression of the quality function can be obtained by substituting (5a), (8), and (9) into (12):

$$\begin{aligned} Q &= \begin{bmatrix} \frac{L}{T_s} \cdot i_d^* + a(k+1) \\ -\frac{L}{T_s} \cdot i_d^i - a(k+1) \end{bmatrix}^2 \\ &\quad + \begin{bmatrix} \frac{L}{T_s} \cdot \frac{2J(\omega^* - \omega(t)) + 2T_{sp} p T_l + 2T_{sp} B \omega(t)}{3 p^2 \psi_f T_{sp}} + b(k+1) \\ -\frac{L}{T_s} \cdot \frac{2J\left(\omega^i - \omega(t)\right) + 2T_{sp} p T_l + 2T_{sp} B \omega(t)}{3 p^2 \psi_f T_{sp}} - b(k+1) \end{bmatrix}^2 \\ &= \left[\frac{L}{T_s} \cdot \left(i_d^* - i_d^i(k+2)\right)\right]^2 \\ &\quad + \left[\frac{2JL}{3 p^2 \psi_f T_s T_{sp}} \cdot \left(\omega^* - \omega^i(t+1)\right)\right]^2 \end{aligned} \tag{13}$$

where $i_d^i(k+2)$ and $\omega^i(t+1)$ represent the predicted d-axis current and predicted speed, respectively. From (13), it can be seen that the speed and current information are included,

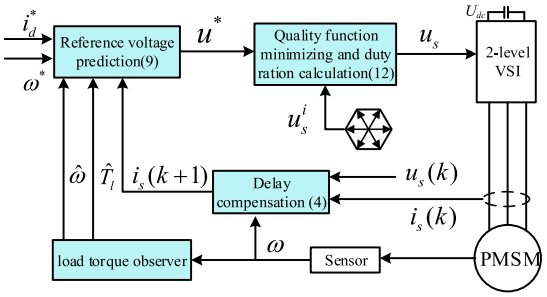

Fig. 1. MP-DSC block diagram.

which means that, although the speed and current need not to be predicted by prediction model in this article, their predictive information can be included in the designed quality function in the form of the difference between the reference voltage vector and candidate voltage vector. In addition, it should be noted that the conventional MPSC method with quality function (10) needs to predict current eight times based on eight basic voltage vectors and then the speed at the next control period is predicted using predicted eight currents. Finally, predicted current and speed are evaluated by the quality function (10). In contrast, in this article, only reference voltage vector needs to be predicted once time in every control period based on reference commands of stator current and speed. Therefore, the computation burden can be effectively reduced, compared with the conventional method.

In this article, in order to achieve better steady-state control performance, the double vector selection principle described in [25] is adopted.

Fig. 1 clearly shows the block diagram of this MP-DSC method, which can be summarized as follows:

1) obtain the load information using load torque observer;
2) compensate one-step delay based on (4);
3) predict the reference voltage vector based on (9);
4) select the optimal voltage vector combination using the quality function (11);
5) set the optimal combination of voltage vectors for the next control period and then return to Step 1).

III. Parameter Sensitivity Analysis of the MP-DSC

From the quality function (11), it is seen that the reference voltage vector u^* directly influence the voltage vector selection. Therefore, in order to obtain the optimal combination of voltage vectors, the reference voltage must be very accurate. However, the motor parameter errors (including the changes of stator resistance, stator inductance, the permanent magnet flux-linkage, viscous friction, and the rotor inertia) and load disturbances will lead to the inaccurate prediction of reference voltage since model (9) needs all these parameters to achieve reference voltage prediction. Thus, it is necessary to evaluate the parameters sensitivity of the MP-DSC method and calculate the error of reference voltage caused by inaccurate model parameters and load disturbance.

Based on model (4), in case of parameter mismatch and inaccurate stator voltage vector $u_{dq}(k)$ reconstruction, the predicted current for delay compensation can be obtained as [16]

$$\begin{cases} i_{de}(k+1) = \left[1 - \frac{T_s(R+\Delta R)}{L+\Delta L}\right] \cdot i_d(k) + T_s\omega(t) i_q(k) \\ \qquad\qquad + \frac{T_s}{L+\Delta L} \cdot u_d(k) + \frac{T_s}{L+\Delta L} \cdot \Delta u_d(k) \\ i_{qe}(k+1) = \left[1 - \frac{T_s(R+\Delta R)}{L+\Delta L}\right] \cdot i_q(k) \\ \qquad\qquad - T_s\omega(t) i_d(k) + \frac{T_s}{L+\Delta L} \cdot u_q(k) \\ \qquad\qquad + \frac{T_s}{L+\Delta L} \cdot \Delta u_q(k) - \frac{T_s\omega(t)(\psi_f+\Delta\psi_f)}{L+\Delta L} \end{cases} \tag{14}$$

where ΔL, $\Delta\Psi_f$, and ΔR represent the errors between nominal and real parameters in the motor model. Δu_d and Δu_q represent the error caused by inaccurate voltage reconstruction. Then current errors between (4) and (14) caused by parameter errors can be obtained as

$$\begin{cases} E_d = i_{de}(k+1) - i_d(k+1) \\ \quad = \frac{T_s R\Delta L - T_s\Delta R L}{L(L+\Delta L)} \cdot i_d(k) - \frac{T_s\Delta L}{L(L+\Delta L)} \cdot u_d(k) \\ \quad + \frac{T_s}{L+\Delta L} \cdot \Delta u_d(k) \\ E_q = i_{qe}(k+1) - i_q(k+1) \\ \quad = \frac{T_s R\Delta L - T_s\Delta R L}{L(L+\Delta L)} \cdot i_q(k) - \frac{T_s\Delta L}{L(L+\Delta L)} \cdot u_q(k) \\ \quad - \frac{T_s\omega(t)}{L(L+\Delta L)}(\psi_f\Delta L + \Delta\psi_f L) + \frac{T_s}{L+\Delta L} \cdot \Delta u_q(k) \end{cases} \tag{15}$$

where E_d and E_q represent the prediction errors of the d-axis current and the q-axis current. Equation (15) indicates that the parameter mismatches (the stator resistance, permanent magnet flux-linkage, and stator inductance) and inaccurate voltage reconstructions directly affect the accuracy of the delay compensation current. In order to simplify analysis, the expression of compensation current under the condition of parameter mismatch and inaccurate voltage reconstruction is shown as follows:

$$\begin{cases} i_{de}(k+1) = i_d(k+1) + E_d \\ i_{qe}(k+1) = i_q(k+1) + E_q \end{cases}. \tag{16}$$

Then, substituting (16) into (9), predicted reference voltage can be obtained asthe following equation as the parameter mismatches, the load disturbance, and inaccurate voltage reconstructions exist:

$$\begin{cases} u_{de}^* = \frac{L+\Delta L}{T_s} \cdot i_d(k+2) + a_e(k+1) \\ u_{qe}^* = \frac{L+\Delta L}{T_s} \cdot \frac{2(J+\Delta J)(\omega^*-\omega(t))+2T_{sp}p(T_l+\Delta T_l)}{3p^2(\psi_f+\Delta\psi_f)T_{sp}} \\ \qquad + \frac{2(B+\Delta B)\omega(t)}{3p^2(\psi_f+\Delta\psi_f)} + b_e(k+1) \end{cases}. \tag{17}$$

In (17),

$$a_e(k+1) = \left(R + \Delta R - \frac{L+\Delta L}{T_s}\right) \cdot i_{de}(k+1) - \omega(t)(L+\Delta L) i_{qe}(k+1);$$

$$b_e(k+1) = \left(R + \Delta R - \frac{L+\Delta L}{T_s}\right) \cdot i_{qe}(k+1) + \omega(t)[(L+\Delta L) i_{de}(k+1) + (\psi_f + \Delta\psi_f)]; u_{de}^*$$

and u_{qe}^* represent the d-axis and q-axis reference voltages after one-step delay compensation; ΔTl is the load disturbance; ΔB is the viscous friction error; and ΔJ is the rotor inertia error.

Similarly, subtracting (17) from (9), reference voltage error caused by parameter mismatches, the load disturbance, and inaccurate voltage reconstructions can be obtained as

$$\begin{cases} D_d = u_{de}^*(k+1) - u_d^*(k+1) \\ \quad = \frac{\Delta L}{T_s} \cdot i_d^* + \Delta a(k+1) \\ D_q = u_{qe}^*(k+1) - u_q^*(k+1) \\ \quad = \frac{1}{T_s} \cdot \left[(L+\Delta L) W_{qe}^* - L W_q^* \right] + \Delta b(k+1) \end{cases} \tag{18}$$

where

$$\begin{aligned} &\Delta a(k+1) \\ &= \left(\Delta R - \frac{\Delta L}{T_s} \right) \cdot i_d(k+1) - \omega(t)[\Delta L i_q(k+1) \\ &\quad + (L+\Delta L) E_q] + (R+\Delta R) E_d - \frac{(L+\Delta L)}{T_s} \cdot E_d; \\ &\Delta b(k+1) \\ &= \left(\Delta R - \frac{\Delta L}{T_s} \right) \cdot i_q(k+1) + (R+\Delta R) E_q - \frac{(L+\Delta L)}{T_s} \\ &\quad \cdot E_q + \omega(t)[\Delta L i_d(k+1) + (L+\Delta L) E_d + \Delta \psi_f]; \\ W_{qe}^* &= \frac{2(J+\Delta J)(\omega^* - \omega(t))}{3p^2(\psi_f + \Delta\psi_f) T_{sp}} + \frac{2(T_l + \Delta T_l)}{3p(\psi_f + \Delta\psi_f)} \\ &\quad + \frac{2(B+\Delta B)\omega(t)}{3p^2(\psi_f + \Delta\psi_f)}; \\ W_q^* &= \frac{2J[\omega^* - \omega(t)]}{3p^2 \psi_f T_{sp}} + \frac{2T_l}{3p\psi_f} + \frac{2B\omega(t)}{3p^2\psi_f}; \end{aligned}$$

and D_d and D_q represent the d-axis and q-axis reference voltage error.

From (18), it can be seen that not only the parameter mismatches and load disturbance but also the inaccurate compensation current have an influence on the reference voltage error. In order to show the independent relationship between each parameter mismatch and the reference voltage error more intuitively, Fig. 2 is given in this article, in which the system operates at the steady state ($\omega^* = \omega = 157$ rad/s; $T_l = 4\,\mathrm{N \cdot m}$; $u_d = -6.5\,\mathrm{V}$; $u_q = 48.79\,\mathrm{V}$; $i_d^* = i_d = 0\,\mathrm{A}$; $i_q^* = i_q = 3.7\,\mathrm{A}$.)

As can be seen from Fig. 2(a), under the condition that other parameter mismatches do not exist, the load disturbance (ΔT_l) only affects the error of the q-axis reference voltage, has no effect on the d-axis reference voltage. Fig. 2(b) indicates that the inductance mismatch (ΔL) has great influence on the error of d-axis reference voltage, but has little influence on the error of q-axis reference voltage, under the condition that other parameter mismatches and load disturbance do not exist. Moreover, from Fig. 2(c) and (d), it can be found that the resistance mismatch (ΔR) and the flux-linkage mismatch ($\Delta \Psi_f$) have a greater impact on the error of the q-axis reference voltage than the error of the d-axis reference voltage. Besides, compared with

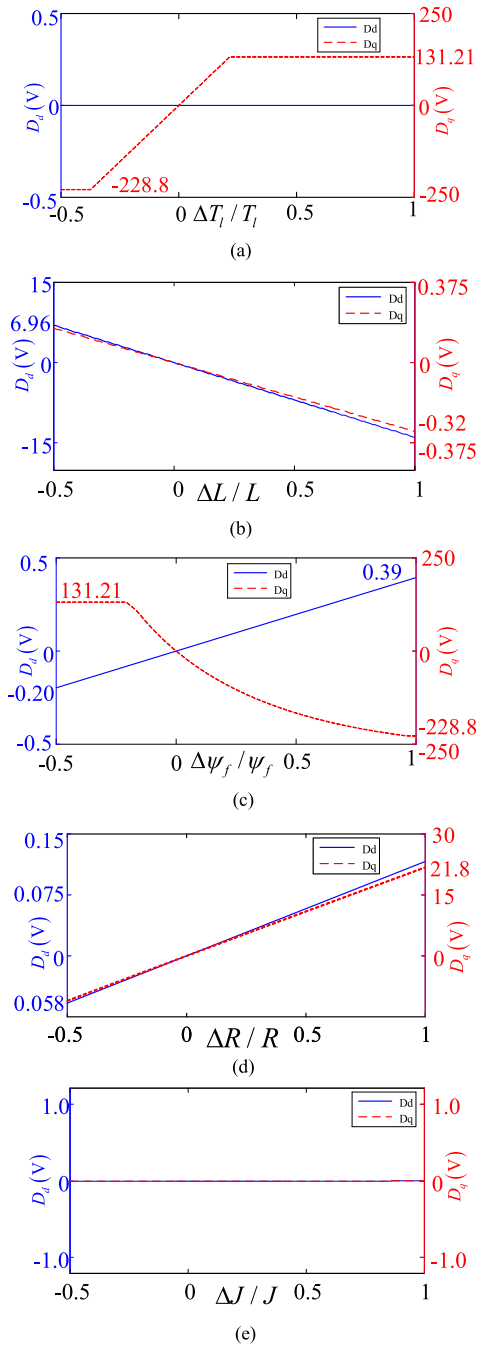

Fig. 2. Relationship between the reference voltage error and the parameter mismatches/load disturbance.

the influence of resistance mismatch, the flux-linkage mismatch makes the error of the q-axis reference voltage larger. In addition, according to the result of Fig. 2(e), it is obvious that the mismatch of moment of inertia does not affect the reference voltage in steady-state conditions.

Above analysis proves that the parameter mismatches and load disturbance have a great influence on the accuracy of reference voltage. Thus, it is very necessary to develop an observer, which can observe the reference voltage error caused by all parameter mismatches and load disturbance.

IV. Proposed FPLO and the MP-DSC+FPLO Method

In this section, a full parameter disturbances and load observer (FPLO) is proposed by using sliding-mode control theory. To obtain the accurate reference voltage vector, the reference voltage error caused by motor parameter mismatches (including electrical parameter mismatches and mechanical parameter mismatch) and load disturbance is simultaneously observed by the FPLO and is compensated online. Thus, the robustness of MP-DSC is improved and the load torque observer in the MP-DSC is omitted.

A. Observer Design

Based on the reference voltage model (9), when the parameter mismatches and load disturbance are taken into account, the reference voltage can be rewritten as

$$\begin{cases} u_d(k) = \frac{L}{T_s}\cdot[i_d(k+1)-i_d(k)] \\ \qquad -\omega(t)Li_q(k+1)+Ri_d(k)+f_d(k) \\ \frac{f_d(k+1)-f_d(k)}{T_s} = F_d \\ u_q(k) = \frac{L}{T_s}\cdot\left[\frac{2J(\omega(t+1)-\omega(t))+2T_{sp}pT_l+2T_{sp}B\omega(t)}{3p^2\psi_f T_{sp}}\right. \\ \qquad \left. -\ i_q(k+1)\right]+\omega(t)\left[Li_d(k)+\psi_f\right]+Ri_q(k+1) \\ \qquad +\ f_q(k) \\ \frac{f_q(k+1)-f_q(k)}{T_{sp}} = F_q \end{cases} \tag{19}$$

where F_d and F_q represent the disturbance variation rates of f_d and f_q, respectively; and f_d and f_q represent all the parameter mismatches and load disturbance, which are expressed as

$$\begin{cases} f_d(k) = \frac{\Delta L}{T_s}\cdot[i_d(k+1)-i_d(k)]+\Delta Ri_d(k)-\Delta u_d(k) \\ \qquad -\omega(t)\left[\Delta Li_q(k+1)+LE_q+\Delta LE_q\right] \\ f_q(k) = \frac{1}{T_s}\left[(L+\Delta L)W_{qe}-LW_q\right. \\ \qquad \left.-\left(\Delta Li_q(k+1)+LE_q+\Delta LE_q\right)\right] \\ \qquad +\omega(t)\left[\Delta Li_d(k)+\Delta\psi_f\right]-\Delta u_q(k) \\ \qquad +\ \left[\Delta R\left(i_q(k+1)+E_q\right)+RE_q\right] \end{cases} \tag{20}$$

where $W_{qe} = \frac{2(J+\Delta J)[\omega(t+1)-\omega(t)]}{3p^2(\psi_f+\Delta\psi_f)T_{sp}} + \frac{2(T_l+\Delta T_l)}{3p(\psi_f+\Delta\psi_f)} + \frac{2(B+\Delta B)\omega(t)}{3p^2(\psi_f+\Delta\psi_f)}$ and $W_q = \frac{2J[\omega(t+1)-\omega(t)]}{3p^2\psi_f T_{sp}} + \frac{2T_l}{3p\psi_f} + \frac{2B\omega(t)}{3p^2\psi_f}$.

From (20), it can be seen that f_d and f_q include full parameter errors (ΔL, $\Delta\Psi_f$, ΔR, ΔB, ΔJ), voltage reconstruction error (Δu_{dq}), load torque error (ΔT_l), and the compensation current error of the q-axis expressed in (15).

For the purpose of observing all the parameter mismatches, voltage reconstruction error, and load disturbance, based on (19), the FPLO observer is proposed as follows:

$$\begin{cases} u_d(k) = \frac{L}{T_s}\cdot\left[\hat{i}_d(k+1)-\hat{i}_d(k)\right]+U_{dsmo} \\ -\omega(t)Li_q(k+1)+R\hat{i}_d(k)+\hat{f}_d(k) \\ \frac{\hat{f}_d(k+1)-\hat{f}_d(k)}{T_s} = \lambda_d\cdot U_{dmso} \\ u_q(k) = \frac{L}{T_s} \\ \quad \cdot\left[\frac{2J(\hat{\omega}(t+1)-\hat{\omega}(t))+2T_{sp}pT_l+2T_{sp}B\hat{\omega}(t)}{3p^2\psi_f T_{sp}}-i_q(k+1)\right] \\ \quad +\hat{\omega}(t)\left[Li_d(k)+\psi_f\right]+Ri_q(k+1)+\hat{f}_q(k)+U_{qsmo} \\ \frac{\hat{f}_q(k+1)-\hat{f}_q(k)}{T_s} = \lambda_q\cdot U_{qsmo} \end{cases} \tag{21}$$

where $\hat{i}_d$ is the estimate value of the d-axis current; $\hat{\omega}$ is an estimate of speed ω; $\hat{f}_d$ and $\hat{f}_q$ are estimate values of f_d and f_q, respectively; coefficient λ_d and λ_q are the sliding-mode parameters; and U_{dsmo} and U_{qsmo} represent the sliding-mode function, respectively.

According to sliding-mode control theory, two key steps need to be completed in the design of the SMO. One step is to design a suitable sliding-mode surface, and another one is to develop a sliding-mode control function (SMCF), which needs to force the estimated variables of SMO to converge to the designed sliding-mode surface. In this article, the speed and current estimation errors are chosen as the linear sliding-mode surfaces, respectively, which are expressed as

$$\begin{cases} S_d = \hat{i}_d - i_d \\ S_\omega = \hat{\omega} - \omega \end{cases} \tag{22}$$

where $\hat{\omega}$ is an estimate value of speed ω, and $\hat{i}_d$ is an i_d estimate value.

It should be noted that the traditional design method of SMCF only cares about whether the system satisfies the stability condition, but not the specific reaching way in which the estimated variables approach the sliding-mode surface. However, the reaching way directly determines the level of the sliding-mode inherent chattering, thus, it has a key impact on the performance of the SMO. In this article, in order to ensure that the estimated variables of the SMO reach the sliding-mode surface quickly with low chattering level, a sliding-mode reaching law expressed by the following equation is designed:

$$\frac{ds}{dt} = -\beta|s|\,\mathrm{sign}(s) \tag{23}$$

where β is the reaching law parameter. In (23), it is obvious that when the estimated speed and current are far from their real values, $|s|$ is large, which means that a faster reaching time to the sliding-mode surface is able to be achieved. On the other hand, when estimated speed and current are near to their real values, $|s|$ gradually become small. which means that when estimated variables approach the sliding-mode surface, the reaching law gradually decreases to zero to suppress the sliding-mode chattering. It can be seen from the above analysis that the proposed observer based on this reaching law can dynamically adapts

to the variations of the sliding-mode surface. Therefore, the inherent sliding-mode chattering can be effectively suppressed.

Then, according to sliding-mode surfaces (22), the discretized equation of reaching law (23) can be obtained as

$$\begin{cases} \frac{s_d(k+1)-s_d(k)}{T_s} = -\beta_d \left|s_d(k)\right| \operatorname{sign}\left(s_d(k)\right) \\ \frac{s_\omega(k+1)-s_\omega(k)}{T_{sp}} = -\beta_\omega \left|s_\omega(k)\right| \operatorname{sign}\left(s_\omega(k)\right) \end{cases}. \tag{24}$$

Next, subtracting (19) from (21), the error equation of this observer can be obtained as follows:

$$\begin{cases} \frac{s_d(k+1)-s_d(k)}{T_s} = -\frac{R}{L}\cdot s_d(k) - \frac{1}{L}\cdot e_{fd}(k) - \frac{1}{L}\cdot U_{d\mathrm{smo}} \\ \frac{e_{fd}(k+1)-e_{fd}(k)}{T_s} = \lambda_d \cdot U_{d\mathrm{smo}} - F_d \\ \frac{s_\omega(k+1)-s_\omega(k)}{T_{sp}} = -\frac{3p^2\psi_f T_s}{2JL}\cdot \begin{bmatrix} s_\omega(k)\left[Li_d(k)+\psi_f\right] \\ +e_{fq}(k) + U_{q\mathrm{smo}} \end{bmatrix} \\ \frac{e_{fq}(k+1)-e_{fq}(k)}{T_{sp}} = \lambda_q \cdot U_{q\mathrm{smo}} - F_q \end{cases} \tag{25}$$

where e_{fd} is the d-axis estimation error, namely, $e_{fd} = \hat{f}_d - f_d$; e_{fq} is the q-axis estimation error, namely, $e_{fq} = \hat{f}_q - f_q$.

Then, substituting (24) into (25), and considering e_{fd}, e_{fq} as disturbances, the SMCF can be designed as

$$\begin{cases} U_{d\mathrm{smo}} = -Rs_d(k) + L\beta_d \left|s_d(k)\right| \operatorname{sign}\left(s_d(k)\right) \\ U_{q\mathrm{smo}} = \frac{2JL\beta_\omega\left|s_\omega(k)\right|}{3p^2\psi_f T_s}\cdot \operatorname{sign}\left(s_\omega(k)\right) - s_\omega(k)\left[Li_d(k)+\psi_f\right] \end{cases}. \tag{26}$$

Finally, the FPLO can be rewritten as the following discrete form:

$$\begin{cases} \hat{i}_d(k+1) = \left(1-\frac{T_s R}{L}\right)\cdot \hat{i}_d(k) + T_s\omega(t) i_q(k+1) \\ \qquad +\frac{T_s}{L}\cdot u_d(k) - \frac{T_s}{L}\cdot \hat{f}_d(k) - \frac{T_s}{L}\cdot U_{d\mathrm{smo}} \\ \hat{f}_d(k+1) = \hat{f}_d(k) + T_s\lambda_d U_{d\mathrm{smo}} \\ \hat{\omega}\,(t+1) = \frac{3p^2\psi_f T_s T_{sp}}{2LJ} \\ \quad \left\{ \begin{array}{l} u_q(k) - \frac{2LT_l}{3p\psi_f T_{sp}} + \left(\frac{L}{T_{sp}} - R\right) i_q(k+1) \\ -\hat{\omega}(t)\left[Li_d(k)+\psi_f\right] - \hat{f}_q(k+1) - U_{q\mathrm{smo}} \end{array} \right\} \\ \quad +\hat{\omega}(t) \\ \hat{f}_q(k+1) = \hat{f}_q(k) + T_{sp}\lambda_q U_{q\mathrm{smo}} \end{cases}. \tag{27}$$

And the block diagram of the proposed FPLO is shown in Fig. 3.

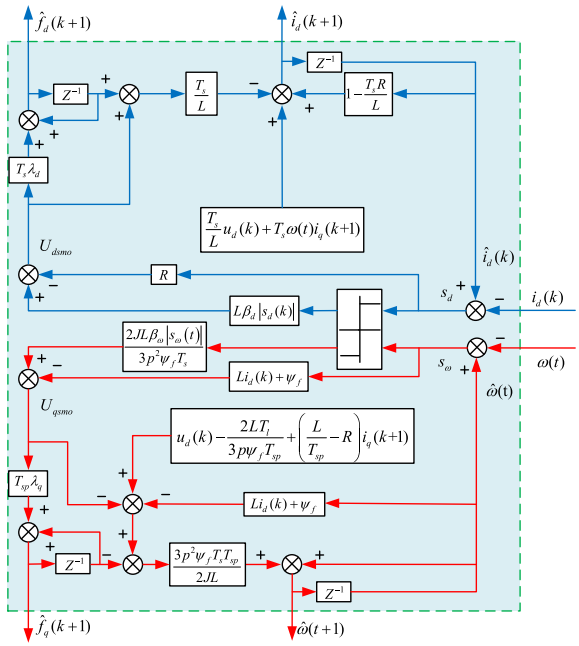

Fig. 3. Block diagram of FPLO.

B. Observer Stability and Parameter Choice

In order to ensure the stability of the designed SMO, the sliding-model parameter should be selected reasonably. Therefore, according to the sliding-mode stability condition, the derivative of the Lyapunov function $V = 1/2s^2$ must keep negative all the time, i.e., $\dot{V} = s\cdot\frac{ds}{dt} < 0$. This means that the following inequalities need to be satisfied based on (25) and (26).

$$s_d\cdot\frac{ds_d}{dt} = s_d(k)\cdot\left(-\frac{R}{L}\cdot s_d(k) - \frac{1}{L}\cdot e_{fd}(k) - \frac{1}{L}\cdot U_{d\mathrm{smo}}\right)$$

$$= s_d(k)\cdot\begin{pmatrix} -\frac{R}{L}\cdot s_d(k) - \frac{1}{L}\cdot e_{fd}(k) \\ +\frac{R}{L}\cdot s_d(k) - \beta_d\left|s_d(k)\right|\operatorname{sign}\left(s_d(k)\right) \end{pmatrix}$$

$$= s_d(k)\cdot\left(-\frac{1}{L}\cdot e_{fd}(k) - \beta_d\left|s_d(k)\right|\operatorname{sign}(s_d(k))\right) < 0$$

$$= \begin{cases} s_d(k)\cdot\left(-\frac{1}{L}\cdot e_{fd}(k) - \beta_d\left|s_d(k)\right|\right) < 0 (s>0) \\ s_d(k)\cdot\left(-\frac{1}{L}\cdot e_{fd}(k) + \beta_d\left|s_d(k)\right|\right) < 0 (s<0) \end{cases}. \tag{28a}$$

$$s_\omega\cdot\frac{ds_\omega}{dt} = -s_\omega(k)\cdot\frac{3p^2\psi_f T_s}{2JL}\cdot\left\{\begin{array}{l} s_\omega(t)\left[Li_d(k)+\psi_f\right] \\ +e_{fq}(k) + U_{q\mathrm{smo}} \end{array}\right\}$$

$$= -s_\omega(k)\cdot\frac{3p^2\psi_f T_s}{2JL}\cdot\left\{\begin{array}{l} s_\omega(t)\left[Li_d(k)+\psi_f\right] + e_{fq}(k) \\ -s_\omega(t)\left[Li_d(k)+\psi_f\right] \\ +\frac{2JL\beta_\omega|s_\omega(t)|}{3p^2\psi_f T_s}\cdot\operatorname{sign}\left(s_\omega(t)\right) \end{array}\right\}$$

$$= -s_\omega(k)\cdot\frac{3p^2\psi_f T_s}{2JL}\cdot\left\{\begin{array}{l} e_{fq}(k) \\ +\frac{2JL\beta_\omega|s_\omega(t)|}{3p^2\psi_f T_s}\cdot\operatorname{sign}\left(s_\omega(t)\right) \end{array}\right\} < 0$$

$$= \begin{cases} -s_\omega(k)\cdot\frac{3p^2\psi_f T_s}{2JL}\cdot\left\{e_{fq}(k) + \frac{2JL\beta_\omega|s_\omega(t)|}{3p^2\psi_f T_s}\right\} < 0 (s>0) \\ -s_\omega(k)\cdot\frac{3p^2\psi_f T_s}{2JL}\cdot\left\{e_{fq}(k) - \frac{2JL\beta_\omega|s_\omega(t)|}{3p^2\psi_f T_s}\right\} < 0 (s<0) \end{cases}. \tag{28b}$$

Then, the selection range of reaching law parameter β can be derived as

$$\begin{cases} \beta_d > \left|\frac{e_{fd}}{L\cdot s_d}\right| \\ \beta_\omega > \left|\frac{e_{fq}}{L\cdot s_\omega}\right| \end{cases}. \tag{29}$$

Thus, the designed SMO with parameter β can reach the sliding-mode surface in a finite time, and stay on it. This means that sliding-mode surface s and its derivative satisfy $s = \frac{ds}{dt} = 0$. Then, error equation (25) can further be simplified as

$$\begin{cases} \frac{e_{fd}(k+1)-e_{fd}(k)}{T_s} + \lambda_d e_{fd}(k) + F_d = 0 \\ \frac{e_{fq}(k+1)-e_{fq}(k)}{T_{sp}} + \lambda_q e_{fq}(k) + F_q = 0 \end{cases}. \tag{30}$$

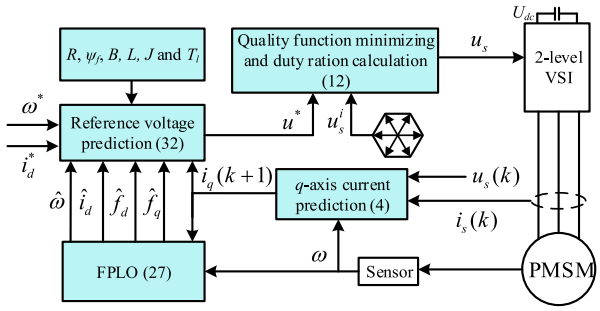

Fig. 4. Structure diagram of the PMSM system based on the proposed MP-DSC+FPLO method.

As a result, the solution (31) of the disturbance estimation errors can be obtained

$$\begin{cases} e_{fd} = e^{-\lambda_d t}\left[K_d + \int F_d \cdot e^{\lambda_d t} dt\right] \\ e_{fq} = e^{-\lambda_q t}\left[K_q + \int F_q \cdot e^{\lambda_q t} dt\right] \end{cases} \tag{31}$$

where K_d and K_q are constants.

Obviously, according to the solution (31), the sliding-mode parametersλ_d and λ_q must be positive to ensure that the disturbance estimation errors e_{fd} and e_{fq} converge to 0.

The above analyses indicate that in order to ensure the stability of the proposed observer, sliding-mode parameters should be selected based on the condition of (29) and (31).

C. MP-DSC+FPLO Method

Based on the proposed FPLO, the predictive reference voltage error caused by parameter mismatches and load disturbance can be obtained easily. Then, the accurate reference voltage prediction can be achieved by compensating this error in real time. Meanwhile, the estimated values $\hat{\omega}$ and $\hat{i}_d$ are employed to replace the measured values ω and i_d of model (9) for better control performance. The compensated reference voltage is expressed as follows:

$$\hat{u}^* = \begin{bmatrix} \hat{u}_d^* \\ \hat{u}_q^* \end{bmatrix} = \begin{bmatrix} \frac{L}{T_s} \cdot i_d^* + \hat{a}(k+1) + \hat{f}_d(k+1) \\ \frac{L}{T_s} \cdot \frac{2J(\omega^* - \hat{\omega}(t)) + 2T_{sp} p T_l}{3p^2 \psi_f T_{sp}} + \hat{b}(k+1) + \hat{f}_q(k+1) \end{bmatrix} \tag{32}$$

where $\hat{a}(k+1) = (R - \frac{L}{T_s}) \cdot \hat{i}_d(k+1) - \hat{\omega}(t) L i_q(k+1)$; $\hat{b}(k+1) = (R - \frac{L}{T_s}) \cdot i_q(k+1) + \hat{\omega}(t)[L\hat{i}_d(k+1) + \psi_f]$

In the implementation of the proposed method, the voltage constraint and current protection must be considered. The current protection of the predictive control strategy based on the vector pre-selection is well reported in [27], and this article adopts this strategy to limit overcurrent. On the other hand, overlarge voltage cannot be outputted in real application, thus the reference voltage needs to be restricted. When the calculated reference voltage exceeds $u_{\mathrm{dc}}/\sqrt{3}$, the following equation is adopted to restrict the reference voltages:

$$\hat{u}^* = \begin{bmatrix} \hat{u}'_d \\ \hat{u}'_q \end{bmatrix} = \begin{bmatrix} \frac{u_{\mathrm{dc}}}{\sqrt{3}} \cdot \frac{\hat{u}_d^*}{\sqrt{(\hat{u}_d^*)^2 + (\hat{u}_q^*)^2}} \\ \frac{u_{\mathrm{dc}}}{\sqrt{3}} \cdot \frac{\hat{u}_q^*}{\sqrt{(\hat{u}_d^*)^2 + (\hat{u}_q^*)^2}} \end{bmatrix}. \tag{33}$$

The control schematic diagram of the MP-DSC+FPLO method is shown in Fig. 4. It should be noted that in practical application, R, ψ_f, B, L, J and T_l as the crude estimations of the true parameters and true load torque should be provided to calculate the reference voltage according to (32).

TABLE I
PARAMETERS OF SPMSM

Motor parameter/symbol	value
DC-bus voltage / U_{dc}	310 V
Rated speed / n_{N}	2000 r/min
Rated torque / T_e	6 N•m
Rated current/ I_N	5.5 A
Number of pole pairs / p	3
Stator phase resistance / R	3Ω
d-and q- axes inductances / L	11mH
Flux linkage / ψ_f	0.24Wb
Rotational inertia / J	0.00129 kg•m^2

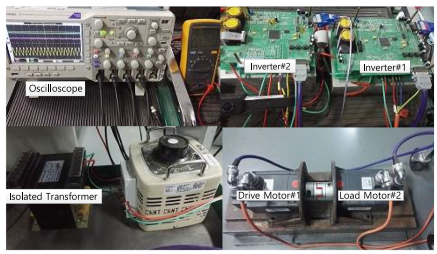

Fig. 5. Photo of the drive platform.

V. EXPERIMENTAL RESULTS

To verify the performance of the proposed method, the experimental tests are performed on an SPMSM drive platform with the TMS320F28335 processor. The sampling frequency used in the experiment is 15 kHz. The main parameters of SPMSM are listed in Table I. the drive platform figure is shown in Fig. 5.

For comparison, the MP-DSC and the conventional model predictive speed control (conventional MPSC) presented in [7] are also implemented. The load torque of these two methods is obtained by an extended sliding-mode load torque observer presented in [26].

The steady-state waveforms of three methods are shown in Figs. 6–10 under the condition of the parameter mismatches and load disturbance. Fig. 6 shows the system responses of three different methods at the condition of 4 N·m load torque. According to the results, all three methods have good steady-state control performance. It should be noted that the proposed method (MP-DSC+FPLO) avoids the application of the load torque observer used in the MP-DSC and conventional MPSC methods since the proposed FPLO can observe parameter disturbances while observing load torque.

Fig. 7 shows the control performances of three control methods under the condition of the 200% inductance mismatch. When the MP-DSC method is applied, speed fluctuation with an amplitude of 15 r/min, d-axis current fluctuation with an amplitude of 1.2 A, and q-axis current fluctuation with an amplitude of 3.8 A exist in the control responses. Similarly, when the conventional MPSC method is used, the speed fluctuation, and the d- and q-axis current fluctuations are 21 r/min, 1.7 A

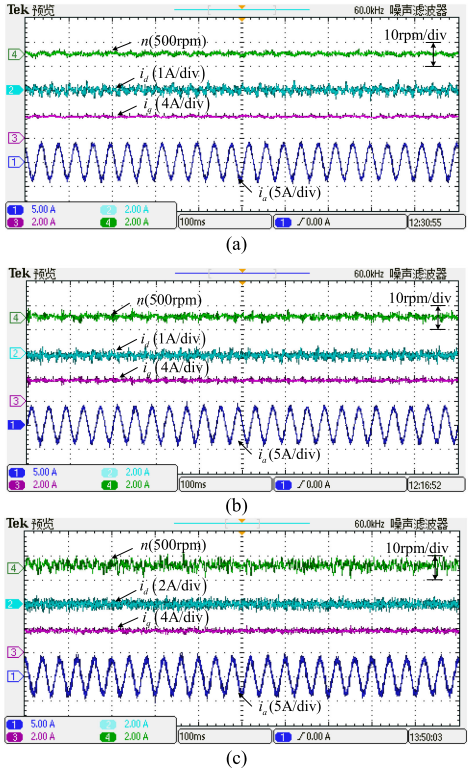

Fig. 6. Experimental results of three methods with 4 N·m load at speed of 500 r/min. (a) MP-DSC+FPLO method. (b) MP-DSC method. (c) Conventional MPSC method.

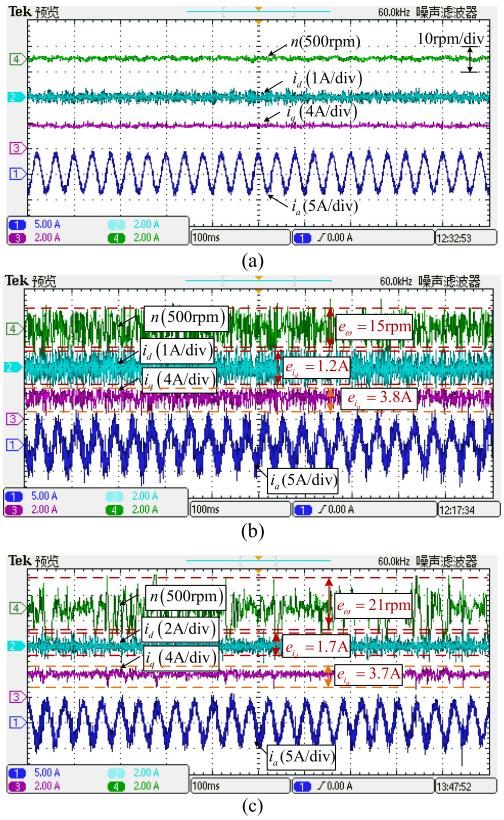

Fig. 7. Experimental results of three methods with 200% error in inductance at speed of 500 r/min. (a) MP-DSC+FPLO method. (b) MP-DSC method. (c) Conventional MPSC method.

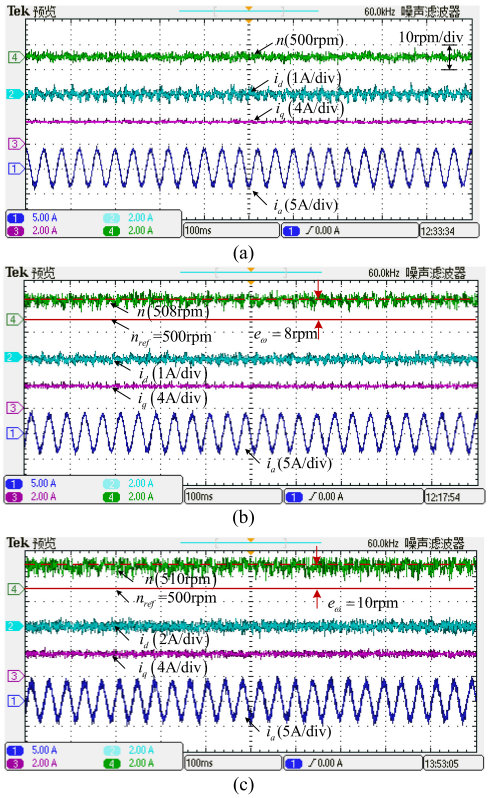

Fig. 8. Experimental results of three methods with 100% error in flux-linkage at speed of 500 r/min. (a) MP-DSC-FPLO method. (b) MP-DSC method. (c) Conventional MPSC method.

and 3.7 A, respectively. However, under the proposed control method, the speed oscillation, *d*-axis current ripple, and the *q*-axis current ripple caused by the inductance mismatch could be well inhibited.

Experimental comparison results of three different methods are shown in Figs. 8 and 9 when flux-linkage mismatch or resistance mismatch exists. From Figs. 8(b), (c) and 9(b) and (c), it can be seen that the flux-linkage mismatch and resistance mismatch result in the speed static error. Fig. 8 indicates, in the case of 100% error in flux-linkage, that the speed static error of the MP-DSC method and the conventional MPSC method reaches 8 r/min and 10 r/min, respectively. On the other hand, when motor resistance in the prediction model increases 200%, the speed static error of the MP-DSC method and the conventional MPSC method reaches 3 r/min and 5 r/min. The resistance mismatch influence on the control performance is smaller than the flux linkage, which further proves the correctness of the theoretical analysis. Compared with the MP-DSC method and conventional MPSC method, it can be found from Figs. 8(a) and 9(a) that the proposed method can achieve speed static-free control no matter under the condition of the flux-linkage mismatch or the resistance mismatch.

The comparison results of the three methods are shown in Fig. 10 when the rotor inertia parameter mismatch exists. The control performances of the three methods have no obvious change at the steady state, which is consistent with the result of parameter sensitivity analysis.

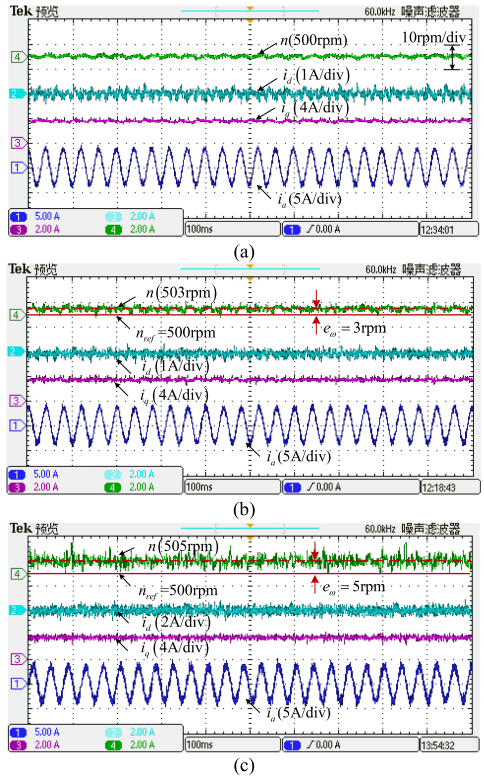

Fig. 9. Experimental results of three methods with 200% error in resistance. (a) MP-DSC-FPLO method at speed of 500 r/min. (b) MP-DSC method. (c) Conventional MPSC method.

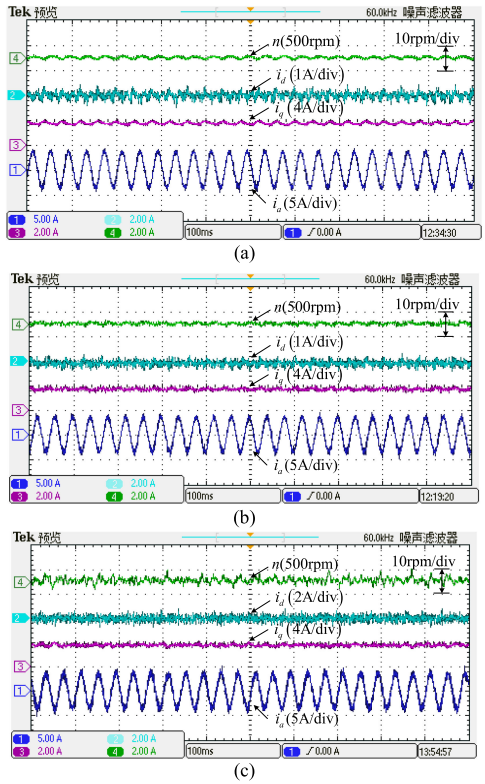

Fig. 10. Experimental results of three methods with 100% error in the rotor inertia at speed of 500 r/min. (a) MP-DSC-FPLO method. (b) MP-DSC method. (c) Conventional MPSC method.

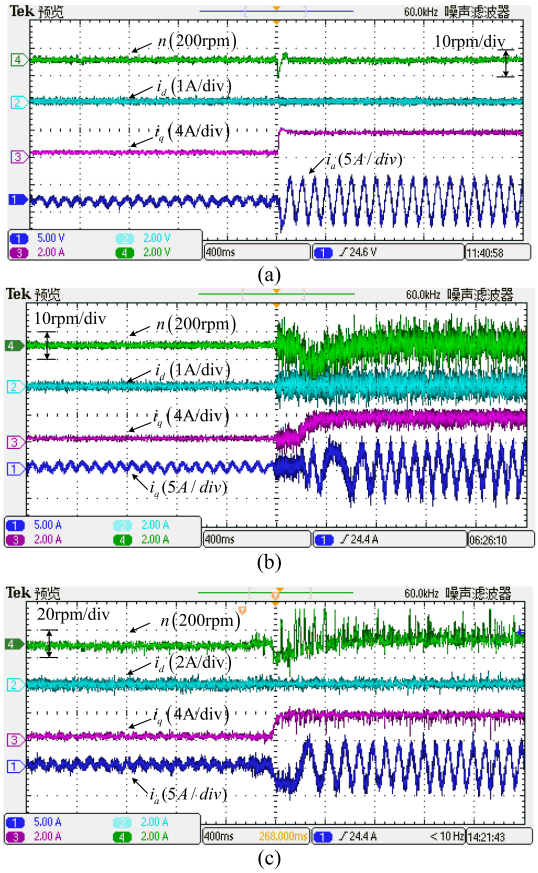

Fig. 11. Experimental results of three methods at 200 r/min when parameter and load change simultaneously. (a) MP-DSC+FPLO method. (b) MP-DSC method. (c) Conventional MPSC method.

In addition to the comparison of steady-state control performance, the dynamic responses of three different methods are also tested in this article under the condition of the parameter mismatch and load change. Figs. 11 and 12 depict the control performance comparisons when load torque and all parameters suddenly change (the inductance parameter changes from 11 to 33 mH, the flux-linkage changes from 0.24 to 0.48 Wb, the resistance changes from 3to 9 Ω, the rotor inertia changes from 0.00129 to 0.00258 kg·m^2, and torque changes from 0 to 4 N·m simultaneously) when the motor operates at 200 r/min and rated speed of 2000 r/min, respectively. It can be seen that the proposed method has better control performance compared with the MP-DSC method and conventional MPSC method.

The comparison results are shown in Fig. 13 when voltage reconstruction errors $u_{dq}(k)$ occur. From the experimental results, it is obvious that similar to parameter mismatches and the load disturbance, inaccurate voltage reconstruction also will deteriorate the control performance of the whole system when the conventional method is applied. However, the proposed method can compensate for this voltage reconstruction error and obtain satisfactory performance. This voltage reconstruction error usually occurs in the one-step delay compensation. This indicates that delay compensation will deteriorate control performances when voltage reconstruction error exists.

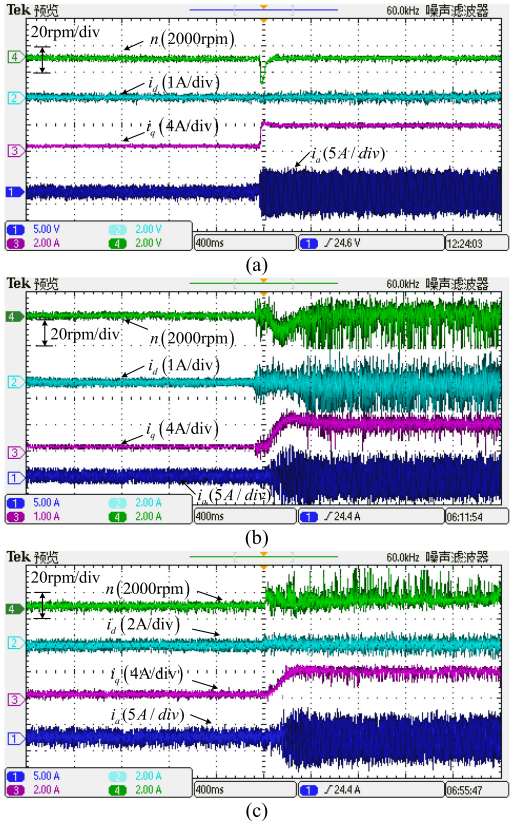

Fig. 12. Experimental results of three methods at rated speed 2000 r/min when parameter and load change simultaneously. (a) MP-DSC+FPLO method. (b) MP-DSC method. (c) Conventional MPSC method.

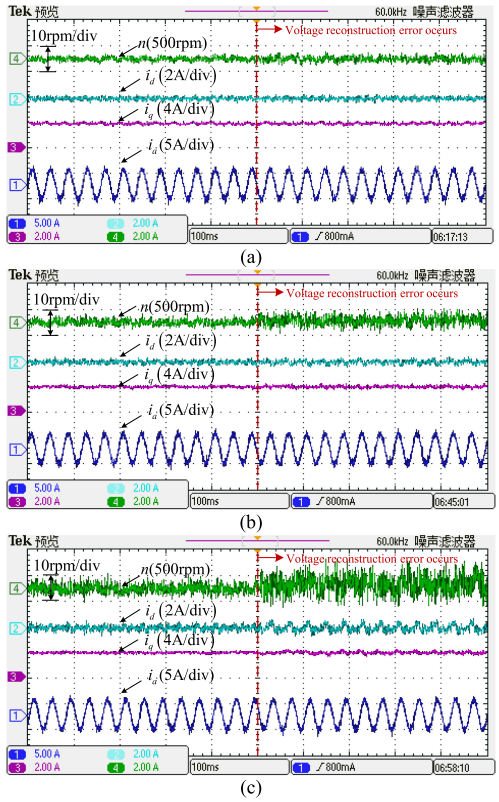

Fig. 13. Experimental results of three methods with 50% error in the voltage reconstruction at the speed of 500 r/min. (a) MP-DSC-FPLO method. (b) MP-DSC method. (c) Conventional MPSC method.

Figs. 14 and 15 show the control performances of the proposed method under different speed and different load torques, when parameter mismatches and load disturbance exist ($\Delta L = 22$ mH, $\Delta\psi_f = 0.24$ Wb, $\Delta R = 6\ \Omega$, $\Delta J = 0.00129$ kg·m^2, and the T_l used in the algorithm is 1 N·m). In Fig. 14, a 4 N·m load torque is suddenly added when the motor operates at the speed of 200 r/min. In Fig. 15, the experimental results of high-speed operation (1500 r/min) are shown, under the condition that a 2 N·m load is suddenly added to the motor. From the results, it can be seen that satisfactory control performance can be obtained with different speed and load.

Finally, the calculation time of the conventional method and the proposed method is compared. The conventional PSC method needs 62.7 μs to complete the whole control algorithm; however, the proposed method only needs 50.63 μs. This indicates that the calculation burden can be reduced by up to 19.2% by adopting the proposed method.

In sum, according to the experimental results, it is obvious that the proposed method reduces the strong dependence of MPC on model parameters (including the mechanical and electrical parameters) and load torque information. Thus, the whole system under the control of the proposed method can keep its strong antidisturbance ability.

In addition, during the algorithm implementation, the authors discover that the parameter of the SMO should be reasonably selected. When the sliding-mode parameter is selected too big, the

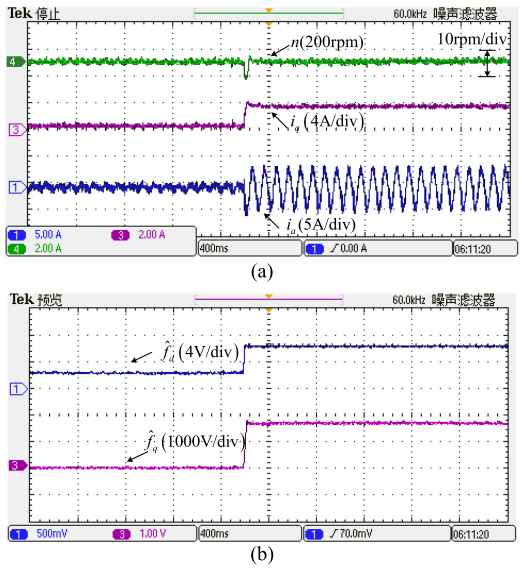

Fig. 14. Experimental results of the MP-DSC-FPLO method at speed of 200 r/min with load sudden change. (a) Speed and current. (b) f_d and f_q estimation.

phenomenon of sliding-mode chattering will be more obvious, and this will affect the system steady-state control performance. When the sliding-mode parameter is selected too small, the convergence characteristic of the sliding mode will be affected. Second, although one-step delay compensation can improve the

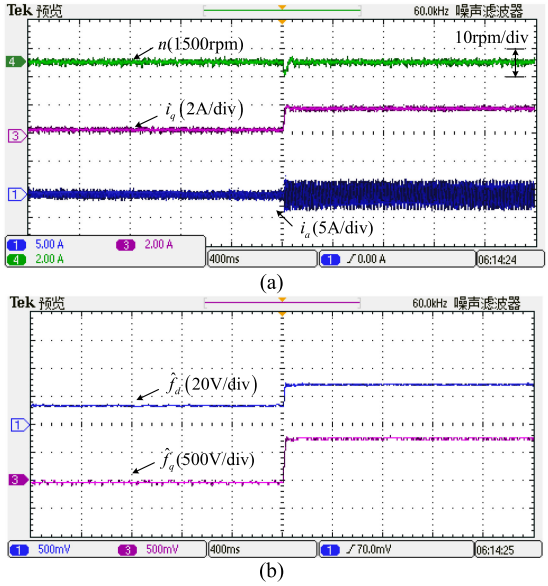

Fig. 15. Experimental results of the MP-DSC-FPLO method at speed of 1500 r/min with load sudden change. (a) Speed and current. (b) f_d and f_q estimation.

control performance according to the existing article report, this issue should be reconsidered when motor parameter mismatches or inaccurate voltage reconstructions exist.

VI. Conclusion

A robust MP-DSC method is proposed and has been experimentally tested. The major contributions of this work include the following. 1) The influence of parameter mismatches and the load disturbance on the speed predictive control performance is analyzed. 2) The FPLO that can simultaneously observe all parameter mismatches (including electrical parameter and mechanical parameter) and torque disturbance is presented. Then, the MP-DSC+FPLO method is developed to improve the antidisturbance ability of the conventional MPSC method.

References

[1] X. Zhu, Z. Xiang, L. Quan, W. Wu, and Y. Du, "Multimode optimization design methodology for a flux-controllable stator permanent magnet memory motor considering driving cycles," *IEEE Trans. Ind. Electron.*, vol. 65, no. 7, pp. 5353–5366, Jul. 2018.

[2] G. Wang, J. Kuang, N. Zhao, G. Zhang and D. Xu, "Rotor position estimation of PMSM in low-speed region and standstill using zero-voltage vector injection," *IEEE Trans. Power Electron.*, vol. 33, no. 9, pp. 7948–7958, Sep. 2018.

[3] Z. Xiang, X. Zhu, L. Quan, Y. Du, C. Zhang, and D. Fan, "Multilevel design optimization and operation of a brushless double mechanical port flux-switching permanent-magnet motor," *IEEE Trans. Ind. Electron.*, vol. 63, no. 10, pp. 6042–6054, Oct. 2016.

[4] G. S. Buja and M. P. Kazmierkowski, "Direct torque control of PWM inverter-fed AC motors - A survey," *IEEE Trans. Ind. Electron.*, vol. 51, no. 4, pp. 744–757, Aug. 2004.

[5] X. Zhang, Y. Li, K. Wang, W. Zhang and D. Gao, " Model predictive control of the open-winding PMSG system based on 3-D reference voltage-vector," *IEEE Trans. Ind. Electron.*, to be published, doi: 10.1109/TIE.2019.2938478.

[6] X. Zhang and K. Wang, "Current prediction based zero sequence current suppression strategy for the semicontrolled open-winding PMSM generation system with a common DC Bus," *IEEE Trans. Ind. Electron.*, vol. 65, no. 8, pp. 6066–6076, Aug. 2018.

[7] E. J. Fuentes, C. A. Silva, and J. I. Yuz, "Predictive speed control of a two-mass system driven by a permanent magnet synchronous motor," *IEEE Trans. Ind. Electron.*, vol. 59, no. 7, pp. 2840–2848, Jul. 2012.

[8] E. Fuentes, D. Kalise, J. Rodríguez, and R. M. Kennel, "Cascade-free predictive speed control for electrical drives," *IEEE Trans. Ind. Electron.*, vol. 61, no. 5, pp. 2176–2184, May 2014.

[9] S. Vazquez, J. Rodriguez, M. Rivera, L. G. Franquelo and M. Norambuena, "Model predictive control for power converters and drives: Advances and trends," *IEEE Trans. Ind. Electron.*, vol. 64, no. 2, pp. 935–947, Feb. 2017.

[10] H. A. Young, M. A. Perez, and J. Rodriguez, "Analysis of finite-control-set model predictive current control with model parameter mismatch in a three-phase inverter," *IEEE Trans. Ind. Electron.*, vol. 63, no. 5, pp. 3100–3107, May 2016.

[11] G. Feng, C. Lai, K. Mukherjee and N. C. Kar, "Online PMSM magnet flux-linkage estimation for rotor magnet condition monitoring using measured speed harmonics," *IEEE Trans. Ind. Appl.*, vol. 53, no. 3, pp. 2786–2794, May/Jun. 2017.

[12] K. Liu and Z. Q. Zhu, "Mechanical parameter estimation of permanent-magnet synchronous machines with aiding from estimation of rotor PM flux linkage," *IEEE Trans. Ind. Appl.*, vol. 51, no. 4, pp. 3115–3125, Jul./Aug. 2015.

[13] L. Niu, M. Yang, and D. Xu, "An adaptive robust predictive current control for PMSM with online inductance identification," *Proc. IREE*, vol. 7, no. 2, pp. 3845–3856, 2012.

[14] K. Liu and Z. Q. Zhu, "Quantum genetic algorithm-based parameter estimation of PMSM under variable speed control accounting for system identifiability and VSI nonlinearity," *IEEE Trans. Ind. Electron.*, vol. 62, no. 4, pp. 2363–2371, Apr. 2015.

[15] M. Yang, X. Lang, J. Long and D. Xu, "Flux immunity robust predictive current control with incremental model and extended state observer for PMSM drive," *IEEE Trans. Power Electron.*, vol. 32, no. 12, pp. 9267–9279, Dec. 2017.

[16] X. Zhang, L. Zhang and Y. Zhang, "Model predictive current control for PMSM drives with parameter robustness improvement," *IEEE Trans. Power Electron.*, vol. 34, no. 2, pp. 1645–1657, Feb. 2019.

[17] H. T. Nguyen and J. Jung, "Finite control set model predictive control to guarantee stability and robustness for surface-mounted PM synchronous motors," *IEEE Trans. Ind. Electron.*, vol. 65, no. 11, pp. 8510–8519, Nov. 2018.

[18] Z. Zhang, Z. Li, M. P. Kazmierkowski, J. Rodríguez, and R. Kennel, "Robust predictive control of three-level NPC back-to-back power converter PMSG wind turbine systems with revised predictions," *IEEE Trans. Power Electron.*, vol. 33, no. 11, pp. 9588–9598, Nov. 2018.

[19] G. Wang, Y. Wang, J. Xu, N. Zhao, and D. Xu, "Weight-transducerless rollback mitigation adopting enhanced MPC with extended state observer for direct-drive elevators," in *IEEE Trans. Power Electron.*, vol. 31, no. 6, pp. 4440–4451, Jun. 2016.

[20] J. Wang, F. Wang, Z. Zhang, S. Li, and J. Rodríguez, "Design and implementation of disturbance compensation-based enhanced robust finite control set predictive torque control for induction motor systems," *IEEE Trans. Ind. Inform.*, vol. 13, no. 5, pp. 2645–2656, Oct. 2017.

[21] B. Wang, X. Chen, Y. Yu, G. Wang, and D. Xu, "Robust predictive current control with online disturbance estimation for induction machine drives," *IEEE Trans. Power Electron.*, vol. 32, no. 6, pp. 4663–4674, Jun. 2017.

[22] C. Xia, M. Wang, Z. Song and T. Liu, "Robust model predictive current control of three-phase voltage source PWM rectifier with online disturbance observation," *IEEE Trans. Ind. Inform.*, vol. 8, no. 3, pp. 459–471, Aug. 2012

[23] X. Zhang, B. Hou, and Y. Mei, "Deadbeat predictive current control of permanent-magnet synchronous motors with stator current and disturbance observer," *IEEE Trans. Power Electron.*, vol. 32, no. 5, pp. 3818–3834, May 2017.

[24] L. Tong *et al.*, "An SRF-PLL-based sensorless vector control using the predictive deadbeat algorithm for the direct-driven permanent magnet synchronous generator," *IEEE Trans. Power Electron.*, vol. 29, no. 6, pp. 2837–2849, Jun. 2014.

[25] X. Zhang and B. Hou, "Double vectors model predictive torque control without weighting factor based on voltage tracking error," *IEEE Trans. Power Electron.*, vol. 33, no. 3, pp. 2368–2380, Mar. 2018.

[26] X. Zhang, L. Sun, K. Zhao and L. Sun, "Nonlinear speed control for PMSM system using sliding-mode control and disturbance compensation techniques," *IEEE Trans. Power Electron.*, vol. 28, no. 3, pp. 1358–1365, Mar. 2013.
[27] Z. Xiaoguang, and H. Yikang, "Direct voltage-selection based model predictive direct speed control for PMSM drives without weighting factor," in *IEEE Trans. Power Electron.*, vol. 34, no. 8, pp. 7838–7851, Aug. 2019.
[28] G. H. B. Foo and M. F. Rahman, "Direct torque control of an IPM-Synchronous motor drive at very low speed using a sliding-mode stator flux observer," *IEEE Trans. Power Electron.*, vol. 25, no. 4, pp. 933–942, Apr. 2010.
[29] Y. Zheng, H. A. A. Fattah, and K. A. Loparo, "Non-linear adaptive sliding mode observer-controller scheme for induction motors," *Int. J. Adapt. Control Signal Process.*, vol. 14, no. 2/3, pp. 245–273, Mar. 2000.
[30] M. Tursini, R. Petrella, and F. Parasiliti, "Adaptive sliding mode observer for speed sensorless control of induction motors," *IEEE Trans. Ind. Appl.*, vol. 36, no. 5, pp. 1380–1387, Sep./Oct. 2000.
[31] J. Davila, L. Fridman, and A. Poznyak, "Observation and identification of mechanical systems via second order sliding modes," *Int. J. Control*, vol. 79, no. 10, pp. 1251–1262, Oct. 2006.
[32] J. Davila, L. Fridman, and A. Levant, "Second-order sliding-mode observer for mechanical systems," *IEEE Trans. Autom. Control*, vol. 50, no. 11, pp. 1785–1789, Nov. 2005.
[33] Y. Feng, X. Yu, and F. Hani, "High-order terminal sliding-mode observer for parameter estimation of a permanent-magnet synchronous motor," *IEEE Trans. Ind. Electron.*, vol. 60, no. 10, pp. 4272–4380, Oct. 2013.

Xiaoguang Zhang (Member, IEEE) received the B.S. degree in electrical engineering from the Heilongjiang Institute of Technology, Harbin, China, in 2007, and the M.S. and Ph.D. degrees in electrical engineering from the Harbin Institute of Technology, Harbin, China, in 2009 and 2014, respectively.

He is currently a Distinguished Professor with the North China University of Technology, Beijing, China. From 2012 to 2013, he was a Research Associate with Wisconsin Electric Machines and Power Electronics Consortium, University of Wisconsin–Madison, Madison, U.S. He has authored or coauthored more than 40 technical papers in the area of motor drives. His current research interests include power electronics and electric machine drives.

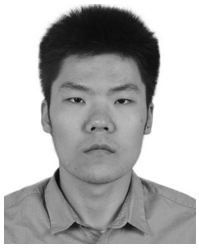

Yu Cheng received the B.S. degree in electrical engineering in 2017 from the North China University of Technology, Beijing, China, where he is currently working toward the M.S. degree.

His current research interests include permanent magnet synchronous motor drives.

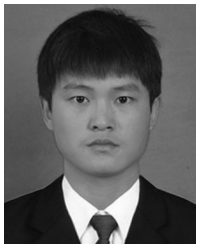

Zhihao Zhao was born in Henan, China, in 1996. He received the B.S. degree in electrical engineering in 2018 from the North China University of Technology, Beijing, China, where he is currently working toward the M.S. degree.

His current research interests include permanent magnet synchronous motor drives.

Yikang He was born in Beijing, China, in 1993. He received the B.S. degree in electrical engineering in 2016 from the North China University of Technology, Beijing, China, where he is currently working toward the M.S. degree.

His current research interests include permanent magnet synchronous motor drives.